

Effects of g -jitter and radiation on three-dimensional double diffusion stagnation point nanofluid flow*

M. H. A. KAMAL, N. A. RAWI, A. ALI, S. SHAFIE†

Department of Mathematical Sciences, Faculty of Science, Universiti Teknologi Malaysia,
Johor Bahru 81310, Johor Darul Takzim, Malaysia

(Received Mar. 14, 2020 / Revised Jul. 21, 2020)

Abstract The unsteady double diffusion of the boundary layer with the nanofluid flow near a three-dimensional (3D) stagnation point body is studied under a microgravity environment. The effects of g -jitter and thermal radiation exist under the microgravity environment, where there is a gravitational field with fluctuations. The flow problem is mathematically formulated into a system of equations derived from the physical laws and principles under the no-slip boundary condition. With the semi-similar transformation technique, the dimensional system of equations is reduced into a dimensionless system of equations, where the dependent variables of the problem are lessened. A numerical solution for the flow problem derived from the system of dimensionless partial differential equations is obtained with the Keller box method, which is an implicit finite difference approach. The effects studied are analyzed in terms of the physical quantities of principle interest with the fluid behavior characteristics, the heat transfer properties, and the concentration distributions. The results show that the value of the curvature ratio parameter represents the geometrical shape of the boundary body, where the stagnation point is located. The increased modulation amplitude parameter produces a fluctuating behavior on all physical quantities studied, where the fluctuating range becomes smaller when the oscillation frequency increases. Moreover, the addition of Cu nanoparticles enhances the thermal conductivity of the heat flux, and the thermal radiation could increase the heat transfer properties.

Key words stagnation point, nanofluid, thermal radiation, g -jitter, double diffusion

Chinese Library Classification O361

2010 Mathematics Subject Classification 76D10, 76E06, 76M20, 76R10

Nomenclature

a ,	principal curvature in the x -direction;	C_{fx} ,	skin friction in the x -direction;
b ,	principal curvature in the y -direction;	C_{fy} ,	skin friction in the y -direction;
C ,	concentration of the fluid;	C_w ,	wall concentration;

* Citation: KAMAL, M. H. A., RAWI, N. A., ALI, A., and SHAFIE, S. Effects of g -jitter and radiation on three-dimensional double diffusion stagnation point nanofluid flow. *Applied Mathematics and Mechanics (English Edition)*, 41(11), 1707–1722 (2020) <https://doi.org/10.1007/s10483-020-2666-6>

† Corresponding author, E-mail: sharidan@utm.my

Project supported by the Ministry of Education (MOE) and Research Management Centre, Universiti Teknologi Malaysia (Nos. 5F166, 5F004, 07G70, 07G72, 07G76, and 07G77)

c_p , specific heat capacity at constant pressure;	Nr , thermal radiation parameter;
C_∞ , nanofluid concentration;	Pr , Prandtl number;
c , curvature ratio;	q_r , nonlinear radiative heat flux;
D , mass diffusion;	Sc , Schmidt number;
f , dimensionless function;	Sh , Sherwood number;
Gr , thermal Grashof number;	T , temperature;
Gm , mass Grashof number;	T_∞ , nanofluid temperature;
g , gravitational field acceleration;	T_w , wall temperature;
g_0 , mean gravitational acceleration;	t , dimensional time;
h , dimensionless function;	t^* , dimensionless parameter of time;
k , thermal conductivity;	u , velocity of the fluid in the x -direction;
k^* , mean absorption coefficient;	v , velocity of the fluid in the y -direction;
Nu , Nusselt number;	w , velocity of the fluid in the z -direction.

Greek symbols

α , thermal diffusion;	ρ , density;
β , thermal expansion;	σ^* , Stefan-Boltzman constant;
β_c , concentration expansion;	τ , dimensionless parameter of time;
ε , the amplitude of modulation;	ϕ , nanoparticles volume fraction;
η , boundary layer thickness;	Φ , dimensionless concentration parameter;
θ , dimensionless temperature parameter;	ω , frequency of oscillation;
μ , dynamic viscosity;	Ω , dimensionless frequency of oscillation.
ν , kinematic viscosity of fluid;	

Scripts

$*$, dimensionless parameter;	f , base fluid;
$'$, differentiation with respect to η ;	s , solid nanoparticle.
nf , nanofluid;	

1 Introduction

The fluid movement affected by viscosity due to the bounding surface is an integral part of fluid mechanics, known as the boundary layer flow^[1]. Studies on boundary layer flow are not only limited to the fluid movement but also include heat transfer properties and concentration distribution, which occur at the thermal and concentration boundary layer^[2]. Theoretical studies on three-dimensional (3D) boundary layer flow with free convection were conducted by Chamkha^[3] and Juel et al.^[4], in which the mathematical modeling was derived from the Navier-Stokes equation. The external force added on the natural force in the flow, namely the mixed convection flow, seems to have a significant effect in most applications since it is widely applied more in manufacturing industries^[5–6]. Fiveland^[7] explored the heat transfer properties either in the fluid or at the boundary layer body for the 3D boundary layer flow with free convection. Lakshmisha et al.^[8] extended the study that covered mass transfer together with heat transfer by explaining the analysis describing the concentration distribution phenomena occurred in the problems. The geometry of a boundary layer body plays a significant part, and the study of the fluid behavior gained researchers' interest to explore^[9]. Since fluids are not only classified as Newtonian, Awais et al.^[10] examined the non-Newtonian fluids which do not obey the Newtonian viscosity characteristics.

A robust physical principle proved the maximal local pressure positioned at stagnation points. The Bernoulli principle gives a very significant reason in considering this effect on boundary layer flow^[11]. Hiemenz^[12] first published the result of a two-dimensional (2D) stagnation-point flow on a boundary layer by utilizing the Navier-Stokes equation in 1911. Later, a large

number of theoretical studies were conducted either in 2D or 3D cases due to its importance to engineering applications^[13–14]. An axisymmetric flow condition was considered in most 3D stagnation point flow problems^[15]. The heat and mass transfer properties on stagnation-point flow were analyzed based on the concentration distribution^[16–17]. Interestingly, for stagnation-point flow cases, the geometry of the boundary body provided very significant results on the flow behavior^[18]. For non-Newtonian fluids, e.g., Casson, second-grade, and third-grade fluids, more parameters were considered in explaining their characteristics and heat transfer properties^[19]. The flow characteristics of non-Newtonian fluids in a stagnation-point region with a magneto-hydrodynamic, porous medium under thermal radiation were also conducted^[20–22].

Thermal radiation is defined as the propagation of thermal electromagnetic particles through a medium^[23]. Rosseland^[24] introduced a nonlinear thermal radiation model that could be applied to boundary layer flow problems. Based on the model presented, Hayat et al.^[25] studied the thermal radiation effect on a 3D boundary layer flow problem. Makinde^[26] investigated the concentration distribution of the free convection flow with thermal radiation and the mass transfer properties of electromagnetic particles past a moving porous plate. Pop et al.^[27] studied the stagnation-point boundary layer problem of flow under thermal radiation.

From the theoretical analysis on the combination of thermal radiation effects with nanofluids for boundary layer problems, it was shown that the thermophysical properties increased by the addition of nanoparticles and heat sources^[28–29]. The thermal radiation effect together with the nanofluid boundary layer flow at a 3D stagnation point region was studied^[30]. The 3D nano-fluid boundary layer flow including gyrotactic microorganisms within a stretching porous cylinder body was numerically studied with the effects of magnetohydrodynamics (MHD), chemical reaction, and thermal radiation^[31].

Nanofluids have been used in many machinery cooling systems due to their excellent performance in transferring heat as compared with classical fluids^[32]. Nanofluids are formed by adding stable microscopic particles with higher thermophysical properties into conventional fluids^[33]. Mansoury et al.^[34] administered an experimental study for the water-based aluminium oxide nanofluid. Zaraki et al.^[35] studied the effects of nanoparticle shape on the heat transfer behaviors of a nanofluid. Rashad et al.^[36] investigated the effects of magnetic field and internal heat generation on a rectangular cavity shape body filled with a saturated porous medium Cu-water nanofluid. For boundary layer problems, there are two popular nanofluid models, i.e., the Buongiorno nanofluid model and the Tiwari and Das nanofluid model^[37–38]. Nanofluids have been applied to either free or mixed 3D boundary layer flows to enhance the thermal conductivity^[39]. The behaviors of 2D^[40–41] and 3D^[18,42] stagnation-point flows under a high static pressure environment were also conducted. Theoretical studies on boundary layer flow under the microgravity environment could show specific flow characteristic behaviors.

Experimental studies were conducted on the assumption of zero gravitational fields at the outer space. It was shown that a pleasant environment existed when a semiconductor was produced without the doping effect and disappeared when small gravitational field disturbance was detected^[43]. The small fluctuating gravitational field, i.e., g -jitter, is caused by crew movement and tremors from mechanical apparatuses in the spacecraft under the microgravity environment^[44]. The literature on the g -jitter effect induced on boundary layer flow is scarce. Nevertheless, some researchers have been able to conduct theoretical studies to analyze the effects of g -jitter on the flow manner^[45–46]. For 2D and 3D stagnation-point flows, the g -jitter effects were studied on the flow pattern and heat transmission, where fluctuating gravitational fields existed^[47–48]. Apart from that, the g -jitter effect together with the thermal radiation induced by the boundary layer flow problem was successfully analyzed, and the results showed a good correlation between the effects considered^[49]. The applications of nanofluids on boundary layer flows induced by the g -jitter effect were also conducted with different types of fluids and geometries^[50–51].

With motivation from the previous research, a fundamental study is conducted on the un-

steady free convection nanofluid flow near a 3D stagnation point region induced by thermal radiation and gravitational modulation. The mathematical model is analyzed in terms of the skin friction coefficient, the Nusselt number, and the Sherwood number, which represent the flow behavior, the heat transfer properties, and the concentration distribution, respectively. The physical explanations for all effects considered in this study are discussed and explained based on the fluid characteristics under certain conditions. The proposed problem has a high potential for engineering applications such as a machinery cooling.

2 Mathematical model

Consider an unsteady incompressible laminar nanofluid flow near a 3D stagnation point embedded in a viscous fluid consisting of Cu nanoparticles and water. At a constant wall temperature and concentration, both the boundary layer flow under a microgravity environment and the thermal radiation are affected by a fluctuating gravitational field. The 3D orthogonal Cartesian coordinate system (x, y, z) is measured along the surface at the nodal point N (see Fig. 1). Initially, the fluid is assumed to move with a constant velocity at the ambient uniform temperature T_∞ and the concentration distribution C_∞ . When the time $t > 0$, the temperature and concentration of the fluid begin to rise to the wall temperature T_w and the body concentration C_w . The stagnation point flow region can be presented as the nodal point N and the saddle point S , which hold the properties of the curvature principle denoted by a and b and are measured at the plane $x = 0$ and $y = 0$. The radiation effect is taken in the energy equation whereby the radiative heat flux is assumed negligible in the x - and y -directions. The physical flow of the nanofluid model near a stagnation point region induced by the g -jitter and thermal radiation into the 3D Cartesian coordinate system is presented in Fig. 1.

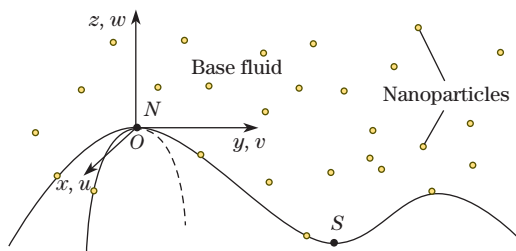


Fig. 1 Physical model of the stagnation point region of the nanofluid flow induced by the g -jitter in the 3D Cartesian coordinates system

Under a microgravity environment, the fluctuating gravitational field behavior, known as the g -jitter effect, is measured as normal to the z -direction depending on t such that

$$g^*(t) = g_0(1 + \varepsilon \cos(\pi\omega t)), \quad (1)$$

where g_0 is the mean of the gravitational acceleration. Meanwhile, ε and Ω are the amplitudes of the modulation and the frequency of oscillation, respectively. By inducing the Tiwari and Das nanofluid model into the 3D Navier-Stokes equation, the governing equation of the incompressible viscous fluid consisting of the continuity, momentum, energy, and concentration equations under the boundary layer and Boussinesq assumptions can be written as follows^[28,38,52]:

$$\frac{\partial u}{\partial x} + \frac{\partial v}{\partial y} + \frac{\partial w}{\partial z} = 0, \quad (2)$$

$$\begin{aligned} & \rho_{\text{nf}} \left(\frac{\partial u}{\partial t} + u \frac{\partial u}{\partial x} + v \frac{\partial u}{\partial y} + w \frac{\partial u}{\partial z} \right) \\ &= \mu_{\text{nf}} \frac{\partial^2 u}{\partial z^2} + g^*(t) (\rho\beta)_{\text{nf}} a x (T - T_\infty) + g^*(t) \rho_{\text{nf}} \beta_c a x (C - C_\infty), \end{aligned} \quad (3)$$

$$\begin{aligned} & \rho_{\text{nf}} \left(\frac{\partial v}{\partial t} + u \frac{\partial v}{\partial x} + v \frac{\partial v}{\partial y} + w \frac{\partial v}{\partial z} \right) \\ &= \mu_{\text{nf}} \frac{\partial^2 v}{\partial z^2} + g^*(t) (\rho\beta)_{\text{nf}} b y (T - T_\infty) + g^*(t) \rho_{\text{nf}} \beta_c b y (C - C_\infty), \end{aligned} \quad (4)$$

$$\frac{\partial T}{\partial t} + u \frac{\partial T}{\partial x} + v \frac{\partial T}{\partial y} + w \frac{\partial T}{\partial z} = \alpha_{\text{nf}} \frac{\partial^2 T}{\partial z^2} - \frac{1}{(\rho c_p)_{\text{nf}}} \frac{\partial q_r}{\partial z}, \quad (5)$$

$$\frac{\partial C}{\partial t} + u \frac{\partial C}{\partial x} + v \frac{\partial C}{\partial y} + w \frac{\partial C}{\partial z} = D_{\text{nf}} \frac{\partial^2 C}{\partial z^2} \quad (6)$$

subject to the following boundary and initial conditions:

$$\begin{cases} t < 0 : u = v = w = 0, & T = T_\infty, & C = C_\infty & \text{for any } x, y, \text{ and } z, \\ t \geq 0 : u = v = w = 0, & T = T_w, & C = C_w & \text{on } z = 0, x \geq 0, y \geq 0; \\ & u = v = w = 0, & T = T_\infty, & C = C_\infty & \text{as } z \rightarrow \infty, x \geq 0, y \geq 0. \end{cases} \quad (7)$$

In the above equations, u , v , and w are the velocity components in the x -, y -, and z -directions, respectively. T and C are the temperature and the concentration, respectively. The script nf corresponds to nanofluid. ρ , μ , β , β_c , α , c_p , and D are denoted as the density, the dynamic viscosity, the thermal expansion, the concentration expansion, the thermal diffusivity, the specific heat capacity at constant pressure, and the mass diffusion, respectively. The principle curvature in the x - and y -directions, represented by a and b , shows the characteristics of the boundary layer flow near a stagnation point region. Based on Rosseland's approximation, the effect of thermal radiation in 3D cases can be simplified into q_r , in which the nonlinear radiative heat flux is defined as follows^[28]:

$$q_r = -\frac{4\sigma^*}{3k^*} \frac{\partial T^4}{\partial z}, \quad (8)$$

where σ^* is the Stefan-Boltzman constant, and k^* is the mean absorption coefficient. The temperature variation is linearized by applying the Taylor series expansion on T^4 to the free stream temperature T_∞ by neglecting higher orders as follows:

$$T^4 \approx 4T_\infty^3 T - 3T_\infty^4. \quad (9)$$

By substituting Eq. (9) into Eq. (8), Eq. (5) can be reduced into

$$\frac{\partial T}{\partial t} + u \frac{\partial T}{\partial x} + v \frac{\partial T}{\partial y} + w \frac{\partial T}{\partial z} = \alpha_{\text{nf}} \frac{\partial^2 T}{\partial z^2} + \frac{1}{(\rho c_p)_{\text{nf}}} \frac{16\sigma^* T_\infty^3}{3k^*} \frac{\partial^2 T}{\partial z^2}. \quad (10)$$

Tiwari and Das's nanofluid model focused on the analysis of the nanoparticle volume fraction and the types of nanoparticles used in the problem. For the viscous Newtonian fluid, the nanofluid constant is derived from Brinkman's equation to define the thermophysical properties

such that^[53-54]

$$\begin{cases} \rho_{nf} = (1 - \phi)\rho_f + \phi\rho_s, & \mu_{nf} = \frac{\mu_f}{(1 - \phi)^{2.5}}, & \alpha_{nf} = \frac{k_{nf}}{(\rho c_p)_{nf}}, \\ (\rho\beta)_{nf} = (1 - \phi)(\rho\beta)_f + \phi(\rho\beta)_s, & (\rho c_p)_{nf} = (1 - \phi)(\rho c_p)_f + \phi(\rho c_p)_s, \\ \frac{k_{nf}}{k_f} = \frac{(k_s + 2k_f) - 2\phi(k_f - k_s)}{(k_s + 2k_f) + \phi(k_f - k_s)}, & D_{nf} = \frac{1 - \phi}{1 + \phi/2}, \end{cases} \quad (11)$$

where ϕ and k are the nanoparticle volume fraction and the thermal conductivity, respectively. The subscripts s and f are solid and fluid, respectively. Cu nanoparticles are added into the base fluid (water) to enhance the thermal conductivity. The values of the thermophysical properties are presented in Table 1^[55].

Table 1 Thermophysical properties for Cu and water^[55]

Thermophysical property	Water	Cu
Density $\rho/(\text{kg}\cdot\text{m}^{-3})$	997.1	8 933
Specific heat capacity $c_p/(\text{J}\cdot\text{kg}^{-1}\cdot\text{K}^{-1})$	4 179	385
Thermal conductivity $k/(\text{W}\cdot\text{m}^{-1}\cdot\text{K}^{-1})$	0.613	400
Thermal expansion coefficient β/K^{-1}	2.1×10^{-4}	1.67×10^{-5}
Thermal diffusion coefficient $\alpha/(\text{m}^2\cdot\text{s}^{-1})$	1.47×10^7	$1.163 1 \times 10^{10}$

As a way to reduce the complexity of the boundary layer problem, a semi-similar transformation technique is applied to the system of partial differential equations in Eqs. (2)–(5) and Eq. (10). As a result, the equations become dimensionless, and the dependent variables are reduced. The semi-similar variables used in this problem are^[48]

$$\begin{cases} \tau = \Omega t^*, & \eta = Gr^{1/4}az, & t^* = va^2Gr^{1/2}t, \\ c = \frac{b}{a}, & \theta(\tau, \eta) = \frac{T - T_\infty}{T_w - T_\infty}, & \Phi(\tau, \eta) = \frac{C - C_\infty}{C_w - C_\infty}, & \Omega = \frac{\omega}{va^2Gr^{1/2}}, \\ u = va^2xGr^{1/2}f'(\tau, \eta), & v = va^2yGr^{1/2}h'(\tau, \eta), & w = -vaGr^{1/4}(f + h), \end{cases} \quad (12)$$

where η and Gr are the kinematic viscosity and the thermal Grashof number, respectively. The dimensional system of Eqs. (2)–(5) and (10) undergoes a semi-similar transformation technique by implementing the nanofluid constant in Eq. (11) and the semi-similar variables in Eq. (12). The present study focuses on the nodal point of attachment. It holds the properties such that $|a| \geq |b|$ and $a \geq 0$. The parameter c is introduced here as the curvature ratio, $c = b/a$, and $0 \leq c \leq 1$ at N . From the literature, the nodal point of attachment holds a characteristic of a general practical body shape such as cylinder and sphere. As a result, the system of the dimensionless equation becomes

$$\begin{aligned} & C_1 f''' + C_2(f + h)f'' - C_2 f'^2 + C_3(1 + \varepsilon \cos(\pi\tau))\theta + \frac{Gm}{Gr}C_2(1 + \varepsilon \cos(\pi\tau))\Phi \\ &= C_2\Omega \frac{\partial f'}{\partial \tau}, \end{aligned} \quad (13)$$

$$\begin{aligned} & C_1 h''' + C_2(f + h)h'' - C_2 h'^2 + cC_3(1 + \varepsilon \cos(\pi\tau))\theta + \frac{Gm}{Gr}cC_2(1 + \varepsilon \cos(\pi\tau))\Phi \\ &= C_2\Omega \frac{\partial h'}{\partial \tau}, \end{aligned} \quad (14)$$

$$\frac{1}{Pr} \left(\frac{C_4 + Nr}{C_5} \right) \theta'' + (f + h) \theta' = \Omega \frac{\partial \theta}{\partial \tau}, \quad (15)$$

$$\frac{1}{Sc} C_6 \Phi'' + (f + h) \Phi' = \Omega \frac{\partial \Phi}{\partial \tau} \quad (16)$$

subject to

$$\begin{cases} f(\eta, 0) = f'(\eta, 0) = 0, & h(\eta, 0) = h'(\eta, 0) = 0, & \theta(\eta, 0) = \Phi(\eta, 0) = 1, \\ f' \rightarrow 0, & h' \rightarrow 0, & \theta \rightarrow 0, & \Phi \rightarrow 0 \quad \text{as } \eta \rightarrow \infty, \end{cases} \quad (17)$$

where

$$\begin{cases} C_1 = \frac{1}{(1 - \phi)^{2.5}}, & C_2 = 1 - \phi + \frac{\phi \rho_s}{\rho_f}, & C_3 = 1 - \phi + \frac{\phi(\rho\beta)_s}{(\rho\beta)_f}, \\ C_4 = \frac{(k_s + 2k_f) - 2\phi(k_f - k_s)}{(k_s + 2k_f) + \phi(k_f - k_s)}, & C_5 = 1 - \phi + \frac{\phi(\rho c_p)_s}{(\rho c_p)_f}, & C_6 = \frac{1 - \phi}{1 + \phi/2}, \\ Pr = \frac{\nu_f}{\alpha_f}, & Nr = \frac{16\sigma^* T_\infty^3}{3k_f k^*}, & Sc = \frac{\nu_f}{D_f}, \\ Gr = \frac{g_0 \beta (T_w - T_\infty)}{a^3 \nu^2}, & Gm = \frac{g_0 \beta_c (C_w - C_\infty)}{a^3 \nu^2}. \end{cases} \quad (18)$$

In the above equations, both the Prandtl number Pr and the Schmidt number Sc are dimensionless. Nr and Gm are the thermal radiation parameter and the mass Grashof number, respectively. The analysis of the problem focuses on the physical quantities of principle interest, which are the skin friction, the Nusselt number, and the Sherwood number. For the skin friction, the flow behavior is analyzed at the x - and y -directions, while the Nusselt number and the Sherwood number focus on the thermal and concentration boundaries, respectively. All dimensional physical quantities of principle interest defined for the nanofluid are written as follows:

$$\begin{cases} C_{fx} = \mu_{nf} \left(\frac{\partial u}{\partial z} \right)_{z=0} / (\rho_f \nu^2 a^3 x), & Nu = -a^{-1} k_{nf} \left(\frac{\partial T}{\partial z} \right)_{z=0} / (k_f (T_w - T_\infty)), \\ C_{fy} = \mu_{nf} \left(\frac{\partial v}{\partial z} \right)_{z=0} / (\rho_f \nu^2 a^3 y), & Sh = -a^{-1} D_{nf} \left(\frac{\partial C}{\partial z} \right)_{z=0} / (D_f (C_w - C_\infty)). \end{cases} \quad (19)$$

By using the same semi-similar variables in Eq. (11) and the nanofluid constant in Eq. (10), the dimensionless physical quantities of principle interest after similarity transformation are

$$\begin{cases} C_{fx}/Gr^{3/4} = f''(\tau, 0)/(1 - \phi)^{2.5}, & C_{fy}/Gr^{3/4} = h''(\tau, 0)/(1 - \phi)^{2.5}, \\ Nu/Gr^{1/4} = -(k_{nf}/k_f)\theta'(\tau, 0) - \theta'(\tau, 0)Nr, & Sh/Gr^{1/4} = -\left(\frac{1 - \phi}{1 + \phi/2} \right) \Phi'(\tau, 0). \end{cases} \quad (20)$$

3 Solution procedure

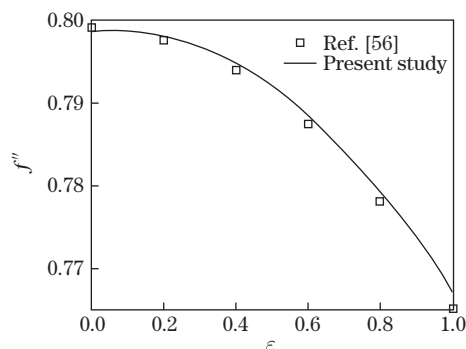
In the previous section, the mathematical modeling of the proposed problem has successfully been reduced into a dimensionless system of equations (see Eqs. (12)–(14)) subjected to the boundary condition in Eq. (15). An implicit finite different procedure is conducted on the system of equations, i.e., the Keller box method. The procedure consists of several steps as follows: (i) to reduce the system of equations into the first-order system, (ii) to discretize the first-order system by using the central difference, (iii) to linearize the obtained results by using

the Newton method, and (iv) to solve the coefficient matrix by using the block tridiagonal matrix^[56]. In the mathematical modeling, the uniform grid with $\Delta\eta = 0.04$ and $\Delta\tau = 0.1$ are used, and the convergence criteria are less than 10^{-10} . The procedure is conducted through the Fortran language platform of Force 2.0 by using a personal computer. The specification of the personal computer is CPU with Intel[®] core[™] i5-2430M CPU @ 2.40 GHz processor and 4.00 GB RAM. The excursion time for the problem to be converged is less than 20 s.

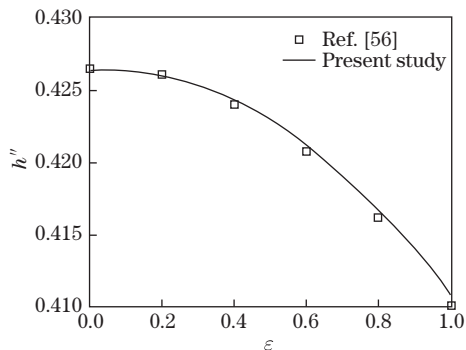
The results of the modulation amplitude, the oscillation frequency size, the nanoparticle volume fraction, the curvature ratio, and the thermal radiation effect are illustrated graphically and critically discussed, respectively. Comparative studies with the published results are also conducted. As shown in Table 2, the results of the present study show satisfactory consistency and accuracy with the results reported in the literature. Figure 2 shows the residual error curves obtained in Ref. [56] and the present study. It can be seen that the published data fit accordingly with the current research.

Table 2 Results of the skin friction coefficient in both directions, the rate of heat flux, and the concentration flux transfer with different values of ε at a small size of Ω , where $\phi = 0$, and $Nr = 0$

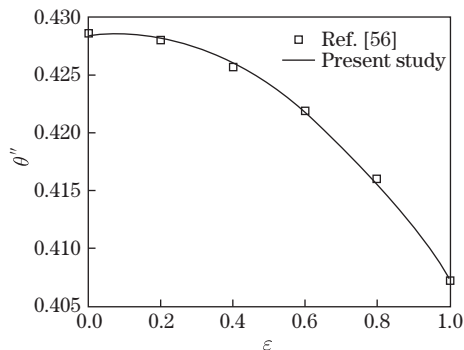
ε	Ref. [56]				Present result			
	f''	h''	θ'	Φ'	f''	h''	θ'	Φ'
0.0	0.799 1	0.426 6	0.428 7	—	0.798 9	0.426 4	0.428 7	0.173 7
0.2	0.797 6	0.426 0	0.428 0	—	0.798 0	0.426 0	0.428 0	0.173 6
0.4	0.794 0	0.424 0	0.425 8	—	0.794 6	0.424 3	0.425 8	0.173 3
0.6	0.787 5	0.420 7	0.421 9	—	0.788 5	0.421 2	0.421 9	0.171 8
0.8	0.778 0	0.416 1	0.416 0	—	0.779 4	0.416 7	0.416 0	0.171 8
1.0	0.765 2	0.410 0	0.407 1	—	0.766 9	0.410 8	0.407 1	0.170 5



(a) Skin friction coefficient in the x -direction



(b) Skin friction coefficient in the y -direction



(c) Rate of heat flux on the wall

Fig. 2 Residual curve error results of the present study and Ref. [56]

3.1 Results and discussion

The flow characteristics, the thermal energy transfer properties, and the mass transfer distribution of this nanofluid flow problem are investigated. The parameter values applied in this research are considered based on the published results and real engineering problems. The effects of the stagnation-point region are analyzed based on the curvature ratio c within the range of $0 < c < 1$. For the modulation amplitude, the values of ε vary from 0 (a steady state) to 1 due to the g -jitter pattern that causes an alternate motion of the gravitational field after $g > 1$. For the oscillation frequency, a single harmonic component Ω is considered. The results are shown in Figs. 3–8, in which there are four subfigures, one for the skin friction coefficient on the x -direction $C_{fx}/Gr^{3/4}$, one for the skin friction coefficient on the y -direction $C_{fy}/Gr^{3/4}$, one for the Nusselt number $Nu/Gr^{1/4}$, and one for the Sherwood number $Sh/Gr^{1/4}$.

The behaviors of the boundary layer flow near a stagnation point region are presented in Figs. 3–5.

In Fig. 3, $c = 0$, $\Omega = 0.2$, $\phi = 0.05$, and $Nr = 1$. From the figure, it is clear that fluctuation behaviors exist for all physical quantities of principle interest except for the skin friction coefficient on the y -direction (see Fig. 3(b)). When $c = 0$, the skin friction coefficient on the y -direction does not have a significant change as the time and the modulation amplitude increase. By selecting $c = 0$, it provides a piece of vital and important information about the geometry at the boundary layer, which is cylindrical. Special types of stagnation point flows occur here as there is no change in terms of the magnitude of the skin friction coefficient. The boundary layer flow produced is known as the plane stagnation-point flow case, since there is no skin friction value change as the parameter τ increases. It can be concluded that a cylindrical geometry surface of $c = 0$ produces the plane stagnation-point flow case.

In Fig. 4, $c = 0.5$, $\Omega = 0.2$, $\phi = 0.05$, and $Nr = 1$. The same fluctuation behaviors are

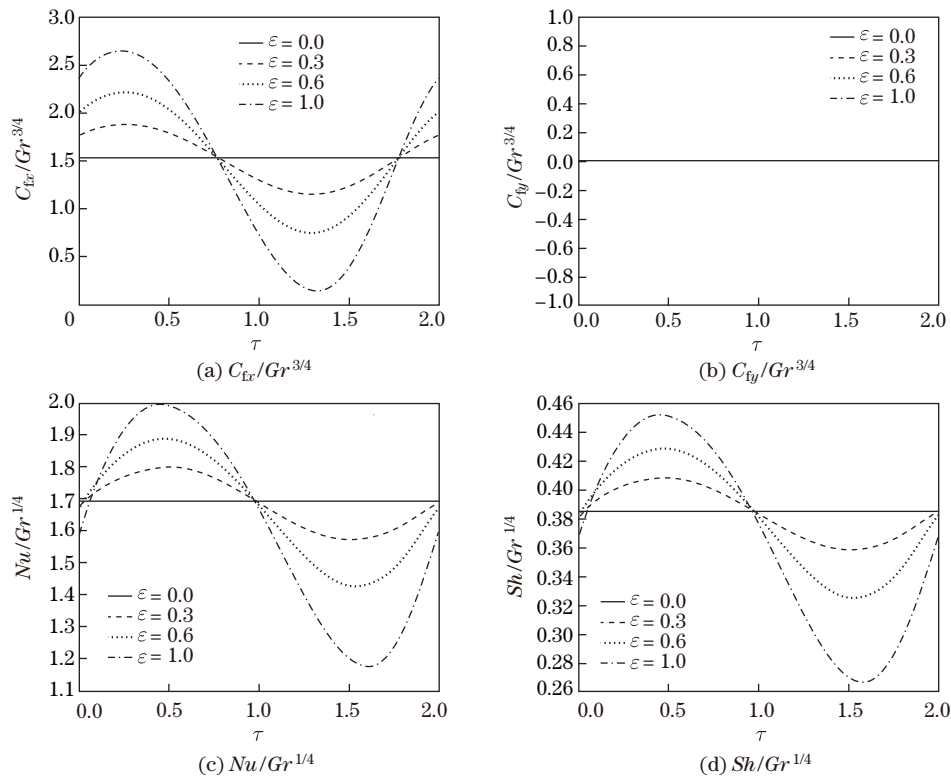


Fig. 3 Physical quantities for $c = 0$, $\Omega = 0.2$, $\phi = 0.05$, $Nr = 1$, and different ε

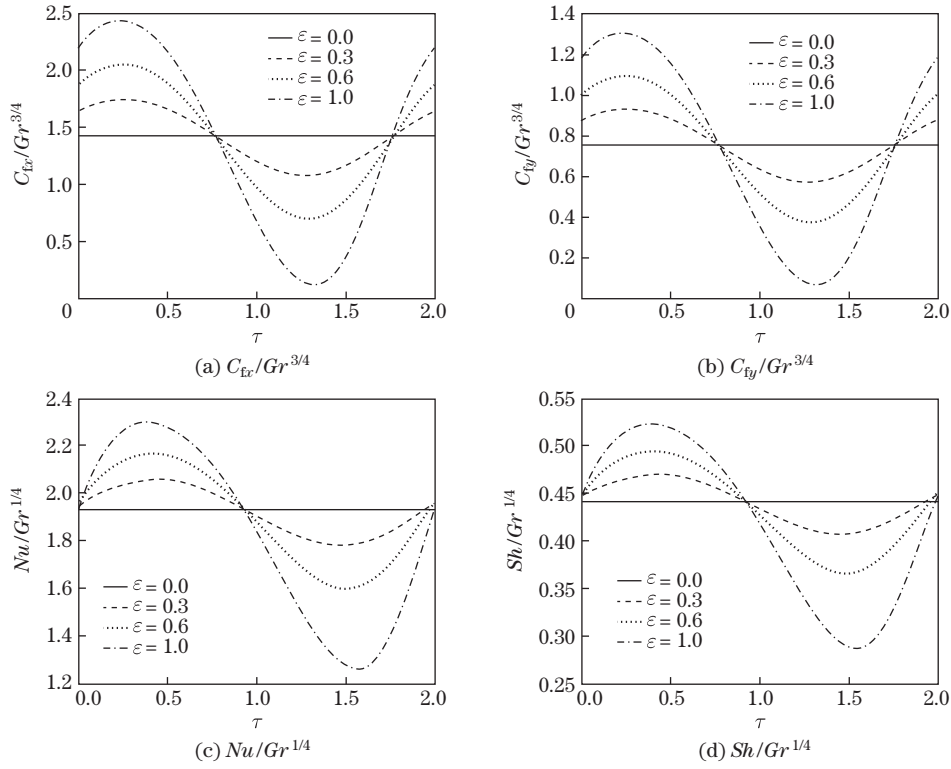


Fig. 4 Physical quantities for $c = 0.5$, $\Omega = 0.2$, $\phi = 0.05$, $Nr = 1$, and different ε

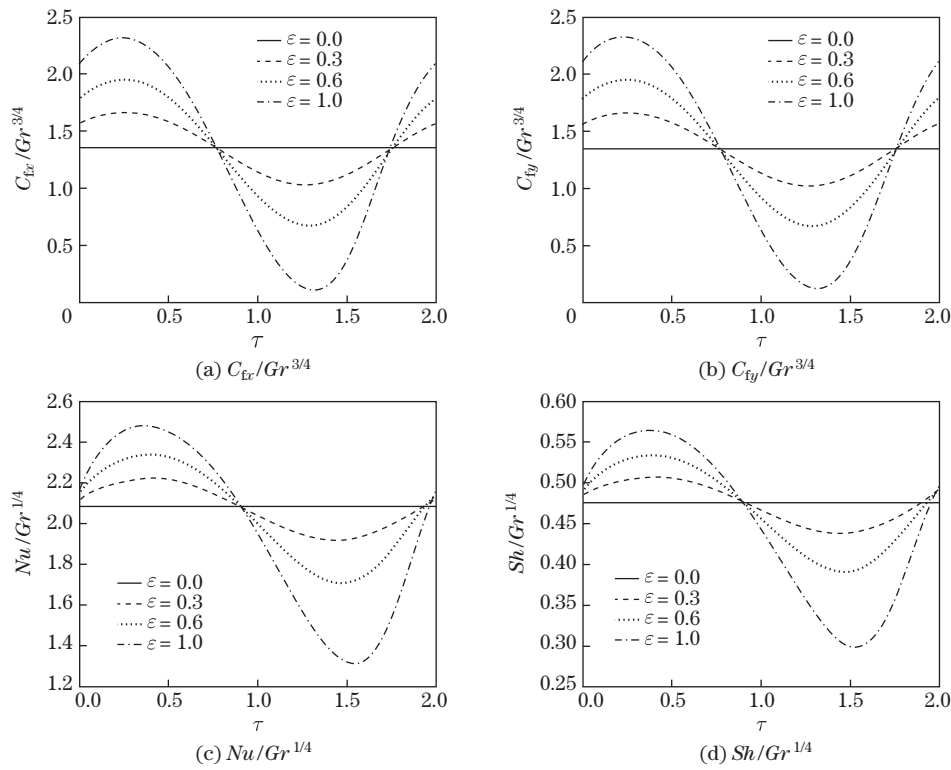


Fig. 5 Physical quantities for $c = 1.0$, $\Omega = 0.2$, $\phi = 0.05$, $Nr = 1$, and different ε

noticed in all physical quantities of principle interest, including the skin friction coefficient in the y -direction which does not change as $c = 0$ in Fig. 3(b). This is because a periodic reversible gravitational field is generated due to the g -jitter effect as ε increases. From Fig. 4, it can be seen that there are the highest and the lowest values in a specified period for all physical quantities of principle interest, and the constant physical quantities only exist at the steady state where $\varepsilon = 0$. Therefore, a small conclusion could be made, i.e., the stagnation point parameter plays a very significant role in the flow behavior.

In Fig. 5, $c = 1$, $\Omega = 0.2$, $\phi = 0.05$, and $Nr = 1$. As shown in the figure, $C_{fx}/Gr^{3/4}$, $C_{fy}/Gr^{3/4}$, $Nu/Gr^{1/4}$, and $Sh/Gr^{1/4}$ show the same behaviors as ε increases, but have different magnitude values. Interestingly, the magnitude values for $C_{fx}/Gr^{3/4}$ and $C_{fy}/Gr^{3/4}$ are the same, which indicates that a particular type of stagnation point flow occurs, which is known as the asymmetry stagnation-point flow case. As the spherical shape of the boundary layer is applied as the boundary body when $c = 1$, the asymmetry stagnation-point flow case is caused by the spherical boundary layer shape.

The effects of the oscillation parameter Ω are analyzed and presented graphically in Fig. 6, in which $c = 0.5$, $\phi = 0.05$, and $Nr = 1$. For each physical quantity of principle interest, different values of Ω provide different results. It can be seen that the effects of Ω on $Nu/Gr^{1/4}$ and $Sh/Gr^{1/4}$ are more significantly than those on $C_{fx}/Gr^{3/4}$ and $C_{fy}/Gr^{3/4}$. As shown in the figure, larger Ω corresponds to larger maximal value for each studied quantity of principle interest for the same value of ε . Lower peak values indicate that the convergence rate of the problem will be more rapid when the frequency of oscillation is larger.

The effects of the nanoparticle volume fraction ϕ on the flow are illustrated in Fig. 7, where $\varepsilon = 0.5$, $\Omega = 0.2$, $Nr = 1$, and $c = 0.5$. It is seen that the values of the skin friction coefficient in both the x - and y -directions increase with in the increase in ϕ . This is due to the additional

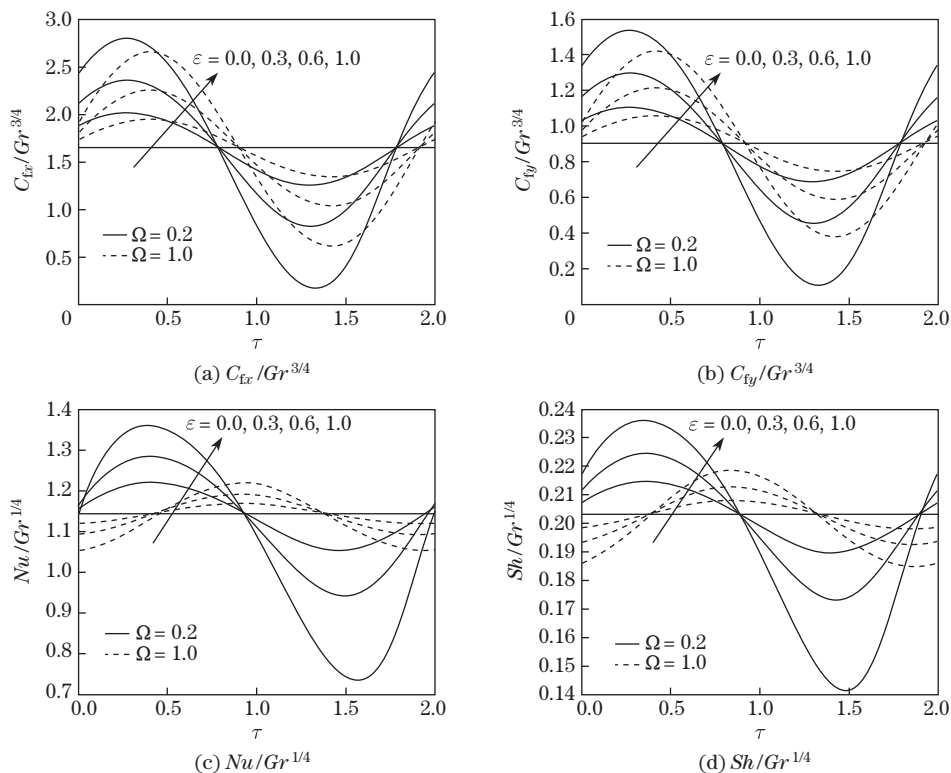


Fig. 6 Physical quantities for different ε and Ω , where $c = 0.5$, $\phi = 0.05$, and $Nr = 1$

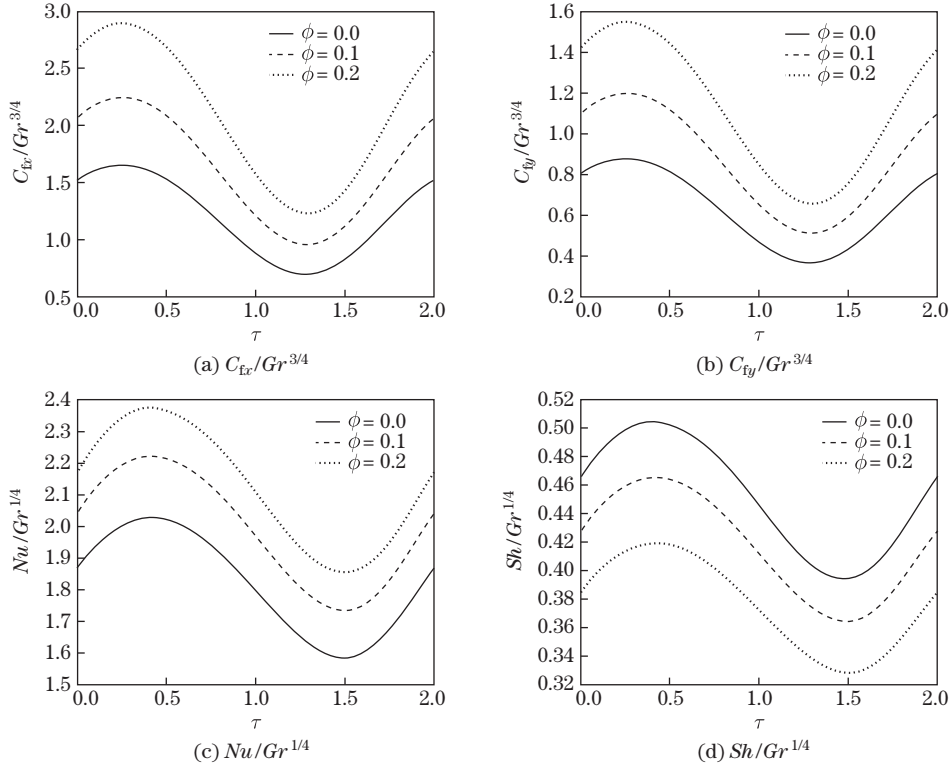


Fig. 7 Physical quantities for different ϕ , where $c = 0.5$, $\Omega = 0.2$, $\varepsilon = 0.5$, and $Nr = 1$

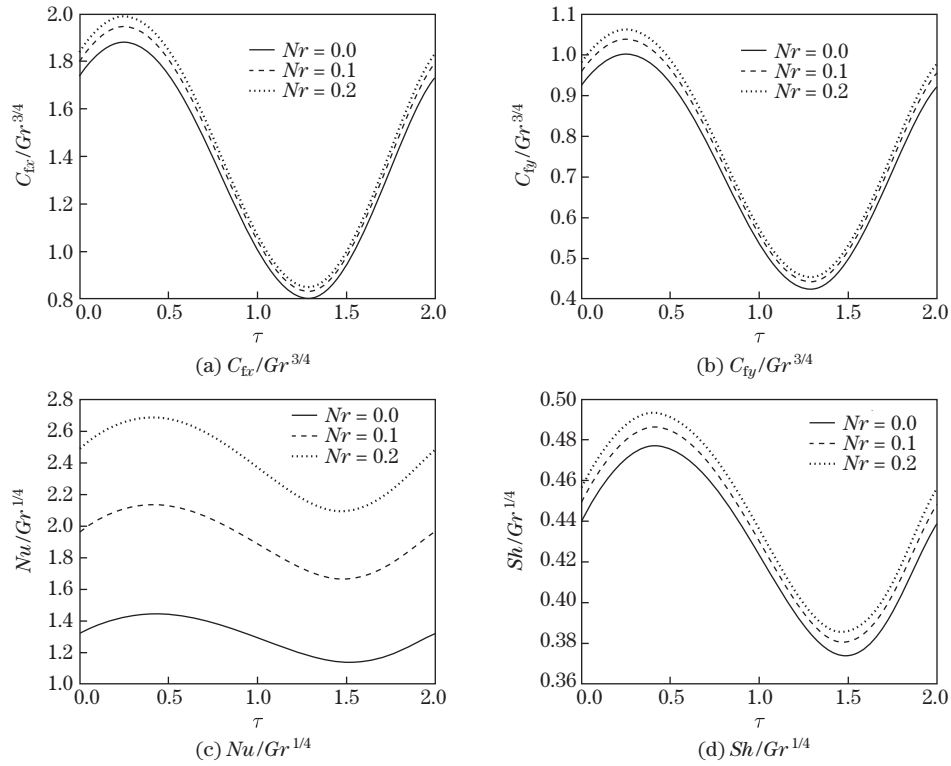


Fig. 8 Physical quantities for different Nr , where $c = 0.5$, $\Omega = 0.2$, $\phi = 0.05$, and $\varepsilon = 0.5$

resistance caused by the nanosize Cu particles in the conventional fluid. The frictional force will then be converted into heat energy, which also enhances the thermal conductivity of the fluid. Besides, the heat transfer properties represented by the Nusselt number show a positive response in terms of the heat conductivity with the addition of Cu nanoparticles in the fluid. Higher thermal conductivity held by Cu nanoparticles causes a fluid enhancement in the heat transfer properties. The results of the Sherwood number are found to decrease as ϕ increases due to the new nanoparticles which enhance the concentration distribution and diffusion in the fluid.

The effects of thermal radiation on the fluid flow characteristics, the thermal energy properties, and the mass dispersion are analyzed in terms of $C_{fx}/Gr^{3/4}$, $C_{fy}/Gr^{3/4}$, $Nu/Gr^{1/4}$, and $Sh/Gr^{1/4}$ are illustrated in Fig. 8. All the analyzed physical quantities show an increased magnitude as the thermal radiation parameter Nr increases. The thermal radiation effect carries the properties of a heat transferring mode occurring in real engineering applications where a more comprehensive system produced is successfully proven in Fig. 8(c). With the consideration of the thermal radiation effect, there is an additional heat created at the main flow domain, particularly at the surface of the heat flux. Thus, $Nu/Gr^{1/4}$ increases as Nr increases. $Nu/Gr^{1/4}$ defines the heat flux on the wall characteristics. With the consideration of the Nr mode of heat transfer, the value of the Nusselt number in the flow increases.

4 Conclusions

The unsteady viscous Newtonian nanofluid with the effects of thermal radiation is successfully studied numerically near a 3D stagnation point body in a fluctuation gravitational field. The Keller box method is implied to solve the mathematical modeling of the proposed problem. The physical quantities of principle interest are implied as indicators in the analysis part. The following highlighted results are obtained.

- (i) Different boundary-layer geometry produces different particular types of stagnation-point flow.
- (ii) The larger the oscillation frequency, the faster the convergence rate.
- (iii) An additional resistance is generated at the boundary surface when the Cu nanoparticles are added into the fluid flow system.
- (iv) The fluid thermal conductivity increases when nanoparticles are added.
- (v) The usage of nanofluid in the flow system does not enhance the concentration properties at the boundary layer.
- (vi) The presence of the thermal radiation effect enhances the heat flux transfer properties at the boundary surface.

Open Access This article is licensed under a Creative Commons Attribution 4.0 International License, which permits use, sharing, adaptation, distribution and reproduction in any medium or format, as long as you give appropriate credit to the original author(s) and the source, provide a link to the Creative Commons licence, and indicate if changes were made. To view a copy of this licence, visit <http://creativecommons.org/licenses/by/4.0/>.

References

- [1] SAKIADIS, B. C. Boundary-layer behavior on continuous solid surfaces, I: boundary-layer equations for two-dimensional and axisymmetric flow. *AIChE Journal*, **7**, 26–28 (1961)
- [2] SUDOH, M., TAKUWA, K., IIZUKA, H., and NAGAMATSUYA, K. Effects of thermal and concentration boundary layers on vapor permeation in membrane distillation of aqueous lithium bromide solution. *Journal of Membrane Science*, **131**, 1–7 (1997)

- [3] CHAMKHA, A. J. Hydromagnetic three-dimensional free convection on a vertical stretching surface with heat generation or absorption. *International Journal of Heat and Fluid Flow*, **20**, 84–92 (1999)
- [4] JUEL, A., MULLIN, T., BEN HADID, H., and HENRY, D. Three-dimensional free convection in molten gallium. *Journal of Fluid Mechanics*, **436**, 267–281 (2001)
- [5] MORGANA, N. O. and LOPEZ, S. E. Numerical simulation of three-dimensional mixed convection in an air-cooled cavity. *Numerical Heat Transfer, Part A: Applications*, **45**, 811–824 (2004)
- [6] MAHANTHESH, B., GIREESHA, B. J., and GORLA, R. S. R. Mixed convection squeezing three-dimensional flow in a rotating channel filled with nanofluid. *International Journal of Numerical Methods for Heat and Fluid Flow*, **26**, 1460–1485 (2016)
- [7] FIVELAND, W. A. Three-dimensional radiative heat-transfer solutions by the discrete-ordinates method. *Journal of Thermophysics and Heat Transfer*, **2**, 309–316 (2004)
- [8] LAKSHMISHA, K. N., VENKATESWARAN, S., and NATH, G. Three-dimensional unsteady flow with heat and mass transfer over a continuous stretching surface. *Journal of Heat Transfer*, **110**, 590–595 (1988)
- [9] MONTGOMERY, D., TURNER, L., and VAHALA, G. Three-dimensional magnetohydrodynamic turbulence in cylindrical geometry. *Physics of Fluids*, **21**, 757–764 (1978)
- [10] AWAIS, M., HAYAT, T., ALSAEDI, A., and ASGHAR, S. Time-dependent three-dimensional boundary layer flow of a Maxwell fluid. *Computers and Fluids*, **91**, 21–27 (2014)
- [11] WANG, C. Y. Stagnation flow towards a shrinking sheet. *International Journal of Non-Linear Mechanics*, **43**, 377–382 (2008)
- [12] HIEMENZ, K. Die grenzschicht an einem in den gleichformigen flüssigkeitsstrom eingetauchten geraden kreiszylinder. *Dinglers Polytech Journal*, **326**, 321–324 (1911)
- [13] JOSEPH, L. N. Incompressible two-dimensional stagnation-point flow of an electrically conducting viscous fluid in the presence of a magnetic field. *Journal of the Aerospace Sciences*, **25**, 194–198 (1958)
- [14] BARIS, S. and DOKUZ, M. S. Three-dimensional stagnation point flow of a second grade fluid towards a moving plate. *International Journal of Engineering Science*, **44**, 49–58 (2006)
- [15] WEIDMAN, P. D. and MAHALINGAM, S. Axisymmetric stagnation-point flow impinging on a transversely oscillating plate with suction. *Journal of Engineering Mathematics*, **31**, 305–318 (1997)
- [16] GERSTEN, K., PAPENFUSS, H. D., and GROSS, J. F. Influence of the Prandtl number on second-order heat transfer due to surface curvature at a three-dimensional stagnation point. *International Journal of Heat and Mass Transfer*, **21**, 275–284 (1978)
- [17] CHAMKHA, A. J. and AHMED, S. E. Similarity solution for unsteady MHD flow near a stagnation point of a three-dimensional porous body with heat and mass transfer, heat generation/absorption and chemical reaction. *Journal of Applied Fluid Mechanics*, **4**, 87–96 (2011)
- [18] UDDIN, M. J., KHAN, W. A., ISMAIL, A. I. M., and BEG, O. A. Computational study of three-dimensional stagnation point nanofluid bioconvection flow on a moving surface with anisotropic slip and thermal jump effect. *Journal of Heat Transfer*, **138**, 1–7 (2016)
- [19] SUBBA, R., GORLA, R., DAKAPPAGARI, V., and POP, I. Boundary layer flow at a three-dimensional stagnation point in power-law non-Newtonian fluids. *International Journal of Heat and Fluid Flow*, **14**, 4008–4012 (1993)
- [20] TURKYILMAZOGLU, M. Three dimensional MHD stagnation flow due to a stretchable rotating disk. *International Journal of Heat Transfer*, **55**, 6959–6965 (2012)
- [21] EL-KABEIR S. M. M. and GORLA, R. S. R. MHD effects on natural convection in a micropolar fluid at a three-dimensional stagnation point in a porous medium. *International Journal of Fluid Mechanics Research*, **34**, 145–158 (2007)
- [22] DEHGHAN, A. A. and BEHNIA, M. Combined natural convection-conduction and radiation heat transfer in a discretely heated open cavity. *Journal of Heat Transfer*, **21**, 56–64 (1996)
- [23] BASU, S., ZHANG, Z. M., and FU, C. J. Review of near-field thermal radiation and its application to energy conversion. *International Journal of Energy Research*, **33**, 56–64 (2009)

-
- [24] ROSSELAND, S. *Astrophysik: Auf Atomtheoretischer Grundlage*, Springer-Verlag, Berlin, 272–276 (1931)
- [25] HAYAT, T., SHEHZAD, S. A., and ALSAEDI, A. Three-dimensional stretched flow of Jeffrey fluid with variable thermal conductivity and thermal radiation. *Applied Mathematics and Mechanics (English Edition)*, **34**(7), 823–832 (2013) <https://doi.org/10.1007/s10483-013-1710-7>
- [26] MAKINDE, O. D. Free convection flow with thermal radiation and mass transfer past a moving vertical porous plate. *International Communication of Heat and Mass Transfer*, **32**, 1411–1419 (2005)
- [27] POP, S. R., GROSAN, T., and POP, I. Radiation effects on the flow near the stagnation point of a stretching sheet. *Technische Mechanik*, **24**, 100–106 (2005)
- [28] HAYAT, T., IMTIAZ, M., ALSAEDI, A., and KUTBI, M. A. MHD three-dimensional flow of nanofluid with velocity slip and nonlinear thermal radiation. *Journal of Magnetism and Magnetic Materials*, **366**, 31–37 (2015)
- [29] HAYAT, T., QAYYUM, S., ALSAEDI, A., and WAQAS, M. Simultaneous influences of mixed convection and nonlinear thermal radiation in stagnation point flow of Oldroyd-B fluid towards an unsteady convectively heated stretched surface. *Journal of Molecular Liquids*, **224**, 811–817 (2016)
- [30] GANESH, K. K., RAMESH, G. K., GIREESHA, B. J., and GORLA, R. S. R. Characteristics of Joule heating and viscous dissipation on three-dimensional flow of Oldroyd B nanofluid with thermal radiation. *Alexandria Engineering Journal*, **57**, 2139–2149 (2018)
- [31] BHATTI, M. M., MISHRA, S. R., ABBAS, T., and RASHIDI, M. M. A mathematical model of MHD nanofluid flow having gyrotactic microorganisms with thermal radiation and chemical reaction effects. *Neural Computing and Applications*, **30**, 1237–1249 (2018)
- [32] RAMESH, G. and PRABHU, N. K. Review of thermo-physical properties, wetting and heat transfer characteristics of nanofluids and their applicability in industrial quench heat treatment. *Nanoscale Research Letters*, **6**, 334–349 (2011)
- [33] CHOI, S. U. S. and EASTMAN, J. A. Enhancing thermal conductivity of fluids with nanoparticles. *ASME International Mechanical Engineering Congress and Exposition*, ASME, San Francisco (1995)
- [34] MANSOURY, D., DOSHMANZIARI, F. I., REZAIE, S., and RASHIDI, M. M. Effect of Al_2O_3 /water nanofluid on performance of parallel flow heat exchangers. *Journal of Thermal Analysis and Calorimetry*, **135**, 625–643 (2019)
- [35] ZARAKI, A., GHALAMBAZ, M., CHAMKHA, A. J., GHALAMBAZ, M., and DE ROSSI, D. Theoretical analysis of natural convection boundary layer heat and mass transfer of nanofluids: effects of size, shape and type of nanoparticles, type of base fluid and working temperature. *Advanced Powder and Technology*, **26**, 935–946 (2015)
- [36] RASHAD, A. M., RASHIDI, M. M., LORENZINI, G., AHMED, S. E., and ALY, A. M. Magnetic field and internal heat generation effects on the free convection in a rectangular cavity filled with a porous medium saturated with Cu-water nanofluid. *International Journal of Heat and Mass Transfer*, **104**, 878–889 (2017)
- [37] BUONGIORNO, J. Convective transport in nanofluids. *Journal of Heat Transfer*, **128**, 240–250 (2006)
- [38] TIWARI, R. K. and DAS, M. K. Heat transfer augmentation in a two-sided lid-driven differentially heated square cavity utilizing nanofluids. *International Journal of Heat and Mass Transfer*, **50**, 2002–2018 (2007)
- [39] SHEREMET, M. A., POP, I., and RAHMAN, M. M. Three-dimensional natural convection in a porous enclosure filled with a nanofluid using Buongiorno's mathematical model. *International Journal of Heat and Mass Transfer*, **82**, 396–405 (2015)
- [40] AKBAR, N. S., KHAN, Z. H., and NADEEM, S. The combined effects of slip and convective boundary conditions on stagnation-point flow of CNT suspended nanofluid over a stretching sheet. *Journal of Molecular Liquids*, **196**, 21–25 (2014)
- [41] BACHOK, N., ISHAK, A., NAZAR, R., and SENU, N. Stagnation-point flow over a permeable stretching/shrinking sheet in a copper-water nanofluid. *Boundary Value Problems*, **1**, 39–49 (2013)

-
- [42] BACHOK, N., ISHAK, A., NAZAR, R., and POP, I. Flow and heat transfer at a general three-dimensional stagnation point in a nanofluid. *Physica B: Condensed Matter*, **405**, 4914–4918 (2010)
- [43] STELIAN, C. and DUFFAR, T. Modeling of a space experiment on Bridgman solidification of concentrated semiconductor alloy. *Journal of Crystal Growth*, **275**, 175–184 (2005)
- [44] BAUMGARTL, J. and MULLER, G. The use of magnetic fields for damping the action of gravity fluctuations (g -jitter) during crystal growth under microgravity. *Journal of Crystal Growth*, **271**, 351–378 (1996)
- [45] FAROOQ, A. and HOMSY, G. M. Streaming flows due to g -jitter-induced natural convection. *Journal of Fluid Mechanics*, **271**, 351–378 (1994)
- [46] YECKEL, A. and DERBY, J. J. Dynamics of three-dimensional convection in microgravity crystal growth: g -jitter with steady magnetic fields. *Journal of Crystal Growth*, **263**, 40–52 (2004)
- [47] REES, D. and POP, I. g -jitter induced free convection near a stagnation point. *Heat and Mass Transfer*, **37**, 403–408 (2001)
- [48] SHAFIE, S., AMIN, N., and POP, I. g -jitter free convection flow in the stagnation-point region of a three-dimensional body. *Mechanics Research Communications*, **34**, 115–122 (2007)
- [49] KAMAL, M. H. A., RAWI, N. A., ILIAS, M. R., ALI, A., and SHAFIE, S. Effect of thermal radiation on a three-dimensional stagnation point region in nanofluid under microgravity environment. *Universal Journal of Mechanical Engineering*, **7**, 272–284 (2019)
- [50] UDDIN, M. J., KHAN, W. A., and AMIN, N. S. g -jitter mixed convective slip flow of nanofluid past a permeable stretching sheet embedded in a Darcian porous medium with variable viscosity. *PLoS One*, **9**, e99384 (2014)
- [51] BHADARIA, B. S., SINGH, A., and KUMAR, V. Nonlinear g -jitter thermal instability in nanofluid in the presence of throughflow and heat source. *Advanced Science, Engineering and Medicine*, **10**, 707–711 (2018)
- [52] KAMAL, M. H. A., ALI, A., and SHAFIE, S. g -jitter free convection flow of nanofluid in the three-dimensional stagnation point region. *Matematika*, **35**, 260–270 (2019)
- [53] OZTOP, H. F. and ABU-NADA, E. Numerical study of natural convection in partially heated rectangular enclosures filled with nanofluids. *International of Heat and Fluid Flow*, **29**, 1326–1336 (2008)
- [54] FENG, X. and JOHNSON, D. W. Mass transfer in SiO₂ nanofluids: a case against purported nanoparticle convection effects. *International Journal of Heat and Mass Transfer*, **55**, 3447–3453 (2012)
- [55] ILIAS, M. R., RAWI, N. A., and SHAFIE, S. MHD free convection flow and heat transfer of ferrofluids over a vertical flat plate with aligned and transverse magnetic field. *Indian Journal of Science and Technology*, **9**, 1–7 (2016)
- [56] SHAFIE, S. *Mathematical Modelling of g -jitter Induced Free Convection*, Ph.D. dissertation, Universiti Teknologi Malaysia, Skudai, 148–149 (2005)